4B.2 RADAR, PROFILER, AND RADIOMETER ANALYSIS OF THE EFFECTS OF MULTIPLE BORES/SOLITARY WAVES ON THE STABILITY OF THE NBL AND ASSOCIATED CI

Timothy A. Coleman*, Kevin R. Knupp, and Dustin Phillips
The University of Alabama, Huntsville, Alabama

1. INTRODUCTION

Atmospheric bores may form when a density current, often produced by other convection, impinges on a stable layer, such as the nocturnal boundary layer (NBL) (e.g., Crook 1988; Rottman and Simpson 1989). It has been shown that atmospheric bores may destabilize the boundary layer through mixing or permanent upward displacements (e.g., Koch et al. 1991), and the lifting may also aide in convective initiation (e.g., Locatelli et al. 2002). Solitary waves or solitons (e.g., Peters and Stoker 1960) may also destabilize the NBL (e.g., Rottman and Einaudi 1993), and may similarly be formed when density currents interact with a stable NBL (e.g., Christie et al. 1978). In this study, multiple bores and solitary waves, initiated by density currents from various convective systems and arriving from different directions, were observed over northern Alabama during the evening hours of 26 June 2008. The wave features passed within 50 km of the UAH ARMOR dual-polarimetric radar, and were also sampled by the UAH Mobile Integrated Profiling System (MIPS), including a 915 MHz wind profiler and a 12-channel microwave profiling radiometer (MPR), located only about 15 km ENE of ARMOR. The main purpose of this study is to quantify the vertical displacements of air parcels by the wave features, and the thermodynamic changes resulting from the destabilizing effects of these features as they pertain to convective initiation. One of the wave features being examined was associated with prolific convective initiation (CI).

Doppler radar reflectivity and velocity data show the bores and waves propagating in the NBL. The 915 MHz wind profiler detected the vertical and horizontal motion perturbations associated with the passing wave features. A time-to-space conversion was performed on the most vigorous wave feature, assuming that the feature was two-dimensional. This allowed for flow trajectories through the wave feature to be calculated, that showed significant vertical displacements (some over 1 km) and vertical spreading of the parcel trajectories within the lowest 2 km AGL. MPR potential temperature calculations showed the vertical spreading of isentropes in two wave features, indicating a decrease in static stability (in some cases, N decreased by more than 50%). Convective parameters including CAPE, CIN, LCL, and LFC were also calculated using MPR temperature and humidity measurements. These measurements clearly showed a decrease in CIN and a lowering of the LFC behind the main wave feature. This decrease in stability and convective inhibition, in addition to the vertical motion associated with the wave, apparently resulted in CI behind the main wave feature.

*Corresponding Author Address: Timothy A. Coleman, Atmospheric Science Department, The University of Alabama in Huntsville, 320 Sparkman Drive, Huntsville, AL 35805; Email: coleman@nsstc.uah.edu.

2. BRIEF REVIEW OF BORES AND SOLITARY WAVES

a. Atmospheric bores

A bore is essentially a hydraulic jump which propagates in a fluid, in which there is a sudden change in depth and fluid motion (Simpson 1997). The energy imbalance at the bore requires that some energy be transferred into the surrounding fluid; in an undular bore, the energy is transported by waves (e.g., Clarke 1972), and in a turbulent bore some of the energy is dissipated through turbulent eddies (Simpson 1997). Atmospheric bores have been examined by many authors (e.g., Tepper 1950; Clarke 1972; Clarke et al. 1981; Crook 1986; Rottman and Simpson 1989). The "morning glory" of the Gulf of Carpentaria in Australia is a classic example of an atmospheric undular bore (e.g., Clarke et al. 1981). Atmospheric undular bores represent a type of gravity wave, and have been shown to produce vertical motions sufficient to generate clouds or convection (e.g., Koch et al. 1991). Bores are accompanied by a rapid and sustained increase in surface pressure associated with the upward displacement and adiabatic cooling, followed by wave-like undulations in the surface pressure; a windshift into the direction of bore motion; and sometimes an increase in surface temperature, caused by mixing in the inversion layer (Koch et al. 1991; Simpson 1997). There is also an associated increase in depth of the stable layer, which is "relatively permanent" (Locatelli et al. 1998), as shown also by Knupp (2006) using potential temperature measurements. A ducting or wave-trapping mechanism may also be necessary for a bore to propagate over a significant distance (e.g., Crook 1986).

Rottman and Simpson (1989) present laboratory measurements that they found to be consistent with atmospheric observations of bores. A likely initiation mechanism for a bore is a density current impinging on a shallow layer of cool, stable air at the surface, such as a temperature inversion (Rottman and Simpson 1989;

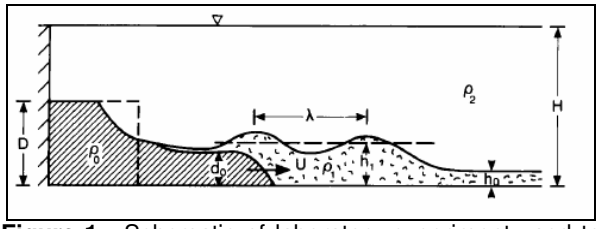

Figure 1. Schematic of laboratory experiment used to generate an undular bore (Rottman and Simpson 1989)

Simpson 1997). A sketch of a laboratory experiment by Rottman and Simpson (1989) representing bore generation through this mechanism is shown (Figure 1). The density current (of depth d_0) initiates a bore in the shallow layer of dense fluid ahead of it. The change in height of the dense fluid (h_1/h_0), known as the bore strength, determines the nature of the bore; when $1 < h_1/h_0 < 2$, the bore is undular, when $2 < h_1/h_0 < 4$, the bore is associated with some mixing, and when $h_1/h_0 > 4$, the bore is turbulent (Rottman and Simpson 1989). The theoretical bore speed may be determined based on the bore strength and the theoretical speed for an internal gravity wave in the surface based layer (C_{gw}). C_{gw} is given by (Simpson 1997):

$$C_{gw} = \left[g\left(\frac{\Delta\theta_v}{\theta_v}\right) h_0 \right]^{1/2} \quad (1)$$

where $\Delta\theta_v$ is the difference in average θ_v between the lower stable layer and the upper layer, and h_0 is the depth of the stable layer. The bore speed (C_{bore}) is then (Rottman and Simpson 1989)

$$C_{bore} = C_{gw}\left[\frac{1}{2}\frac{h_1}{h_0}\left(1+\frac{h_1}{h_0}\right)\right]^{1/2} \quad (2)$$

Laboratory experiments done by Rottman and Simpson (1989) and atmospheric measurements by Clarke et al. (1981) indicate that, for bore strengths between 1.0 and 2.0, the horizontal wavelength of the waves behind the bore should be about 10(+/- 4) * h_1.

The vertical displacements of air as a bore passes may be significant. Koch et al. (1991) combined Raman lidar and radiosonde data to produce an estimate of the change in the vertical structure of potential temperature associated with the passage of a bore (Figure 2). In this case, bore passage was around 0300 UTC. Note the large vertical displacement of some isentropes, that roughly represent air parcel displacements in the absence of evaporation or condensation. For example, the 306 K isentrope in Figure 2 is displaced upward by about 1400 m in about 45 minutes. The isentropes then seem to oscillate, probably indicating the undular nature of the bore, after 0300 UTC.

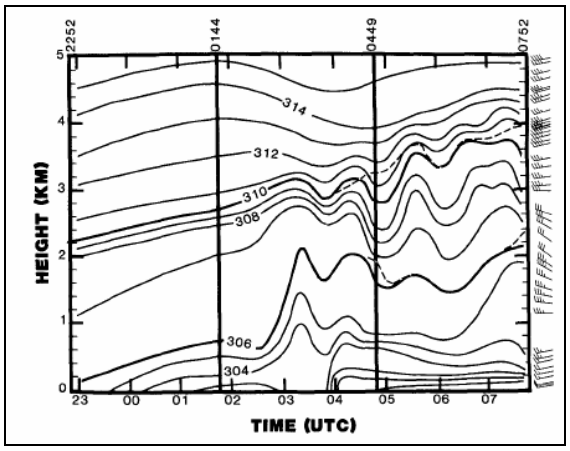

Figure 2. Time-height cross section of potential temperature associated with the passage of a bore and a density current (Koch et al. 1991)

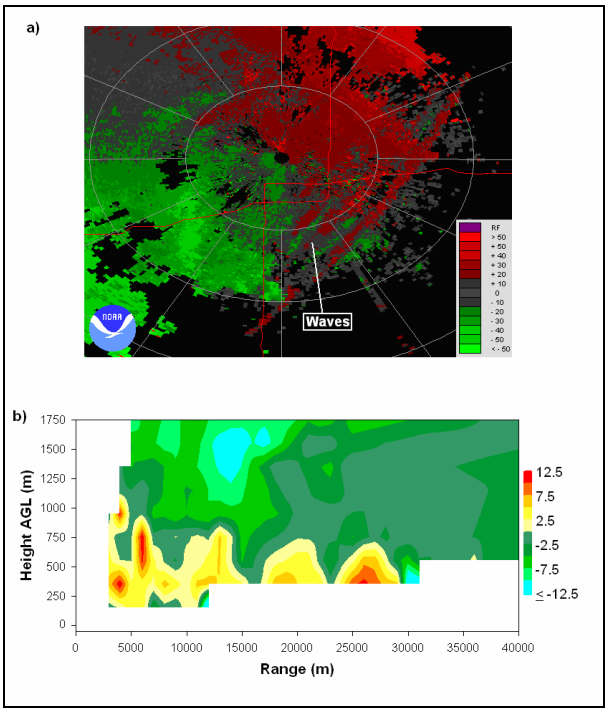

Figure 3. a) PPI radial velocity (knots) from DMX WSR-88D at 1458 UTC on 2 October 2007. Note the undulations in velocity behind the leading edge of the bore. b) Vertical cross-section of radial velocity (m s^{-1}) from DMX at 140 degrees azimuth, at 1450 UTC.

The upward motion associated with the leading edge of a bore implies convergence. Radar observations of an undular bore over Iowa on 2 October 2007 (Coleman et al. 2009) provide an excellent sample of the horizontal winds associated with the bore and its undulations, and the convergence. Figure 3 shows a PPI scan of radial velocity associated with the bore at 1458 UTC, and a cross-section of radial velocity normal to the bore at 1450 UTC. Large outbound velocities, near 10 m s^{-1}, are located at the leading edge of the bore, that is between 25 and 30 km range. These are followed by waves, with peak-to-peak velocity amplitudes of 7.5 to 10 m s^{-1}. There is also fairly large convergence near the leading edge of the bore. Convergence at 30 km range was significant, calculated near 2 x 10^{-2} s^{-1}.

b. Solitary waves

A solitary wave is typically a single wave of elevation, propagating at uniform velocity (e.g., Lamb 1932; Christie et al. 1978; Simpson 1997). They may exist at the interface of two fluids with different density (such as a temperature inversion) (Simpson 1997), and typically produce a temporary increase in surface pressure (Simpson 1997), due to the temporary

increase in the depth of the stable layer (Figure 4). Solitary waves may be generated when density currents, such as thunderstorm outflows, interact with a stable layer (e.g., Christie et al. 1978; Doviak and Ge 1984). The equations governing solitary waves in shallow water were derived first (Boussinesq 1871; Rayleigh 1876). These authors found that the fluid height varies according to the square of the hyperbolic secant of *x*, when *x* = 0 at the center of the wave (maximum amplitude). Then, internal solitary waves were examined (e.g., Abdullah 1956). Benjamin (1967) and Davis and Acrivos (1967) derived equations for internal solitary waves in fluids of great depth, such as those in the atmosphere (Christie et al. 1978). The relative amplitude is $\alpha = a/h$, where *a* is the maximum amplitude of the wave, and *h* is the depth of the undisturbed stable layer. The speed of the wave is then given by (e.g., Christie et al. 1978)

$$c = \left(g \frac{(\rho_1 - \rho_2)}{\rho_1} h \right)^{1/2} \left(1 + \frac{3}{4} \alpha \right)^{1/2} \qquad (3)$$

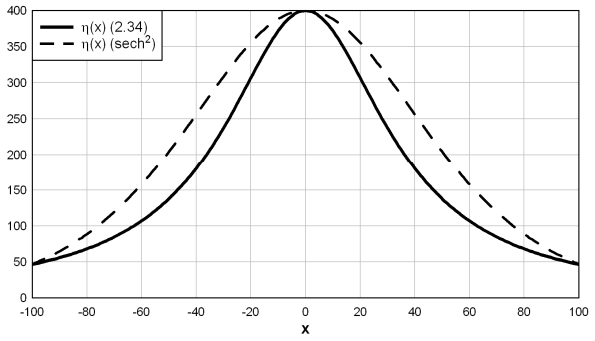

Figure 4. Vertical displacement of solitary wave using theory (solid curve) and the square of the hyperbolic secant (dashed curve) (from Coleman 2008).

3. SYNOPTIC/MESOSCALE ENVIRONMENT

On 26 June 2008, northern and central Alabama were located in a surface ridge, and under extremely light winds aloft (less than 10 m s^{-1} at 500 hPa and 300 hPa). Conditions were seasonably favorable for pulse-type convection on 25-26 June, especially over central Alabama, with low vertical wind shear, surface-based CAPE values at 00 UTC of 1,000 to 2,000 J kg^{-1}, precipitable water values of 2.5 to 3.75 cm, and a very weak 500 hPa shortwave approaching from the northwest.

Scattered convection developed over much of Alabama between 25/18 UTC and 26/00 UTC, with convection persisting well after sunset. An 0200 UTC PPI reflectivity scan at 0.7 degrees elevation from the UAH ARMOR radar (Figure 5) indicates two primary areas of convection: one extended from southern Tennessee into northwest Alabama, west and northwest of the radar at 75 to 100 km range, and the other was

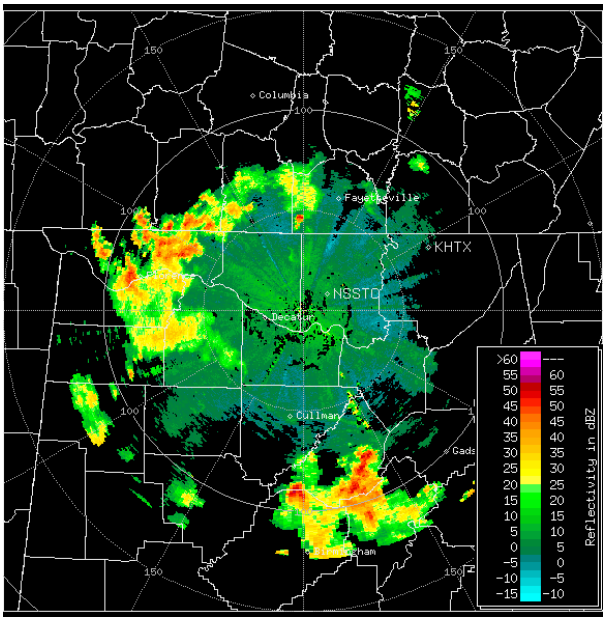

Figure 5. ARMOR reflectivity (dBz) at 0.7 degrees elevation at 0200 UTC. The maximum range of data shown is 125 km. All ARMOR images herein are at 0.7 degrees elevation.

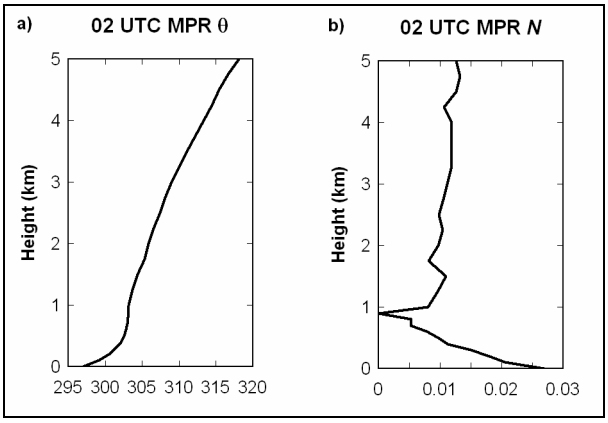

Figure 6. MPR-derived vertical profiles of a) potential temperature (K) and Brunt-Vaisala frequency (s^{-1}).

located in north-central Alabama, SSE of the radar at 85 to 125 km range. Both areas of convection were weakening around 0200 UTC, and they were moving very slowly north to northeastward at about 5 m s^{-1}.

A pronounced low-level stable layer was present at 0200 UTC at NSSTC, as evidenced by microwave profiling radiometer (MPR) data (Figure 6). The stable layer extended from the surface to about 400 m AGL, with Brunt-Vaisala frequencies in this layer between 0.015 and 0.030 s^{-1}. The inversion was topped by a much less stable layer above about 500 m AGL, with a near adiabatic lapse rate (*N* = 0) at 1 km AGL, and *N* near 0.01 s^{-1} through most of the layer between 1 and 5 km AGL. This provided a duct for gravity wave energy (e.g., Lindzen and Tung 1976; Nappo 2002).

4. OVERVIEW OF WAVE FEATURES

a. Wave feature 1 – Undular bore

The first significant wave feature, an undular bore, passed over the UAH instrument suite around 0225 UTC. The bore was approaching from the NW, and is shown fairly well as an alternating inbound/outbound velocity signature from the ARMOR Doppler radar as early as 0144 UTC (Figure 7). Radar at 0144 UTC shows the bore front and 1.5 wavelengths of undulations behind it, with wavelengths around 5 km.

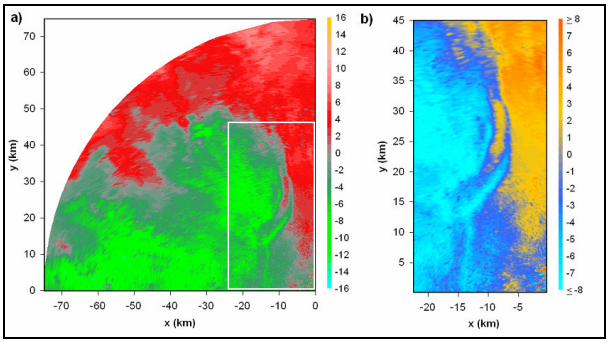

Figure 7. a) ARMOR Doppler velocity image (NW quadrant only) showing undular bore NNW of radar site at 0144 UTC, b) zoomed and color-enhanced velocity at the same time in box shown in panel a.

The undular bore arrived at UAH around 0225 UTC, causing an abrupt but small 0.25 hPa pressure jump in 3 minutes, followed by slowly oscillating and rising pressure. It is notable that, after bore passage, surface temperature rose slightly (about 1 degree C) and surface dewpoint dropped slightly (about 1 degree C), consistent with the passage of a bore, as opposed to an outflow boundary, that would cause a drop in temperature and typically a rise in dewpoint.

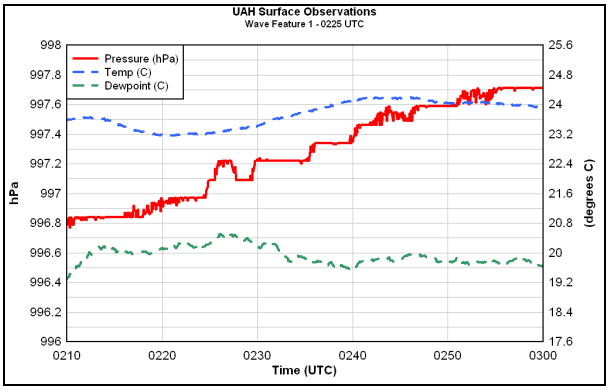

Figure 8. UAH 5-second surface observations of pressure (hPa, solid red), temperature (C, dashed blue), and dewpoint (C, dashed green), around the time of the first bore passage at 0225 UTC.

The bore developed additional undulations by the time it reached the UAH MIPS site around 0225 UTC. A time-height section of vertical motion from the MIPS 915 MHz Doppler wind profiler (Figure 9) shows 4 full-wavelength oscillations in vertical motion between 0225 and 0241 UTC. The first vertical motion couplet was the strongest and deepest vertically, extending above 1500 m AGL, with a maximum upward motion of 1.49 m s^{-1} and a maximum downward motion of 2.17 m s^{-1}. A plot of vertical motion at 400 m AGL vs. time is also in Figure 9, and clearly shows 4 wavelengths in vertical motion.

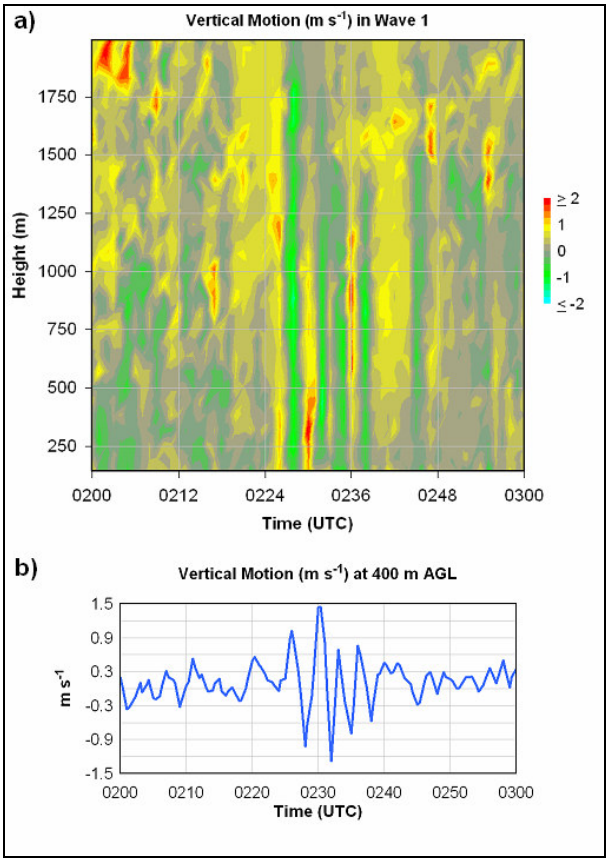

Figure 9. a) Time-height section of MIPS 915 MHz profiler vertical motion, and b) plot of vertical motion vs. time at 400 m AGL (along horizontal blue line in a).

The vertical motion associated with the bore, and its effects on the vertical temperature and moisture profile in the atmosphere, are shown by UAH MIPS MPR (Microwave Profiling Radiometer) data. The potential temperature θ is calculated using temperature data from the MPR directly, and derived pressure using the hypsometric equation. The same derived pressure is used along with temperature and the equation of state to calculate density, allowing water vapor density to be changed to water vapor mixing ratio (r_v). Time-height sections of water vapor mixing ratio and potential temperature are shown in Figure 10 for 0200-0300 UTC. Since ceilometer data and the relatively high lifted condensation levels (LCL) indicate that no evaporation

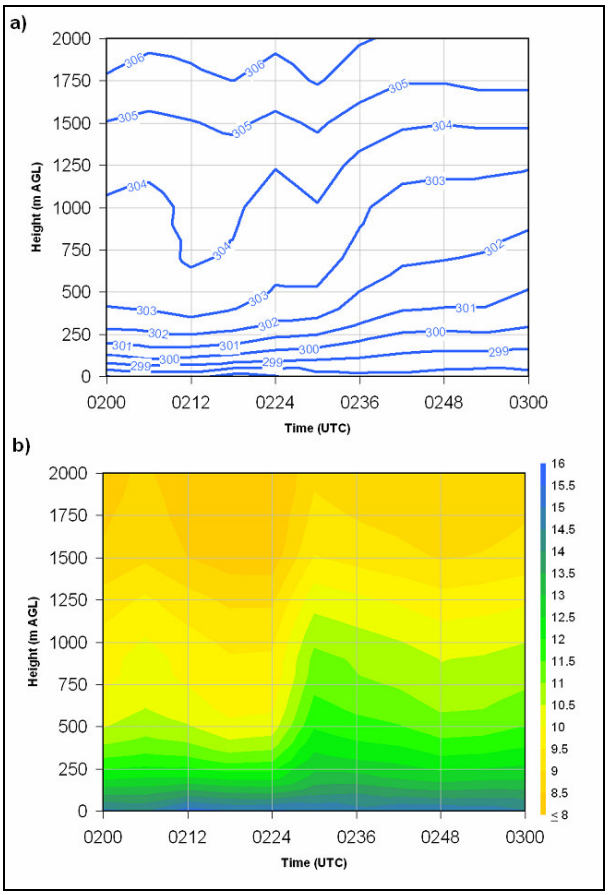

Figure 10. Time height sections of a) potential temperature (K) and b) water vapor mixing ratio (g kg^{-1}) between 0200 and 0300 UTC from UAH MPR data.

nor condensation were occurring during this timeframe, θ and r_v were conserved during vertical motion, and therefore serve as indicators of parcel displacements.

The sudden increase in the depth of the nocturnal boundary layer (NBL) associated with the passage of the bore is apparent in Figure 10. The 303 K isentrope, seeming to indicate the top of the nocturnal inversion, jumps from around 400 m AGL at 0219 UTC to 1100 m AGL by 0240 UTC. The 10.5 g kg^{-1} mixing ratio contour, also at 400 m AGL before bore passage, jumps to about 1150 m AGL very quickly after the bore passes the site at 0225 UTC. These observations indicate that the height of the NBL before the passage of the bore, h_0, was about 400 m AGL, and the NBL height after the bore, h_1, was about 1100 m, indicating a bore strength h_1/h_0 of 2.75. Using equations 1 and 2, along with the mean potential temperature in and above the pre-bore NBL, indicate that the theoretical bore speed would be c_{bore} = 14.2 m s^{-1}. ARMOR radar data indicate the actual speed of the disturbance was 12.2 m s^{-1}, very close to the theoretical bore speed. The speed of the bore may have been decreased slightly due to slight background headwinds (see Figure 7). It should also be noted that vertical mixing associated with the bore destabilized the NBL, as the isentropes spread vertically upon passage of the bore. This destabilization will be discussed in more detail in section 5.

b. Wave feature 2 – Solitary wave/soliton

Intense convection was ongoing at 0130 UTC 75 to 125 km SSE of the ARMOR radar location, near and northeast of Birmingham, Alabama (see Figure 11). Cold outflow from these storms, in the form of a density current, moved northward from these storms, and initiated a wave feature to the SSE of the radar between 0200 and 0300 UTC (see Figure 12). This feature moved generally northward at an average speed of 8 m s^{-1} through 0300 UTC, then sped up to almost 20 m s^{-1} between 0300 and 0400 UTC. This is characteristic of a density current to bore to soliton transition (e.g., Knupp 2006). Upon examination of equations 2 and 3, and the speed of a density current (e.g., Seitter 1986), given the same density difference between the stable NBL and the layer above, amplitude of the feature, and other relevant parameters, the speed of a bore is greater than that of a density current, and the speed of a solitary wave is faster than that of a bore.

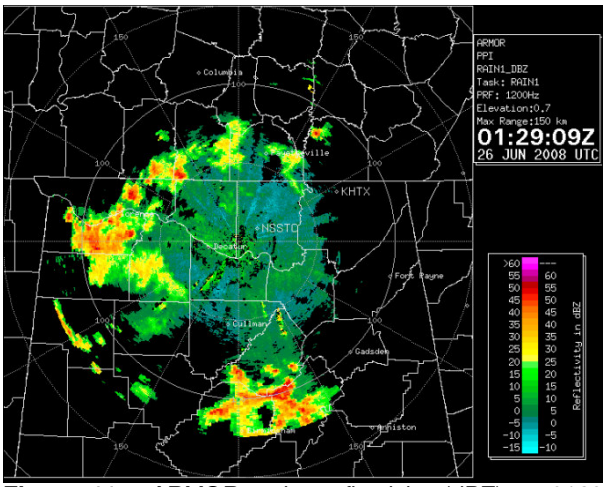

Figure 11. ARMOR radar reflectivity (dBZ) at 0129 UTC.

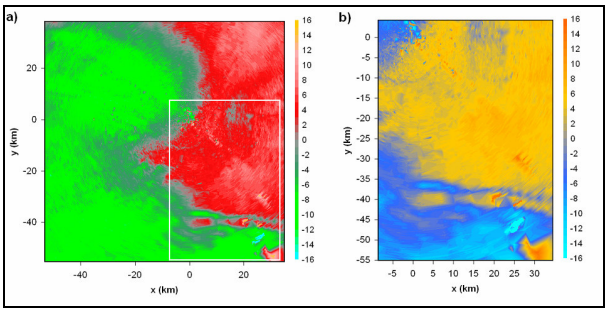

Figure 12. a) ARMOR Doppler velocity image showing wave feature SSE of radar site at 0228 UTC, b) zoomed and color-enhanced velocity at the same time in box shown in panel on left.

The wave evolved into a soliton, or a train of two solitary waves, with the first having the most significant vertical motion. As shown in Figure 13, the period of the vertical motion oscillations was significantly longer for the second wave feature than for the bore around 0225 UTC. There was a sustained period of upward vertical velocities at the UAH MIPS 915 MHz profiler site from about 0352 UTC to about 0407 UTC, followed by shorter periods of downward and then upward motion. At the surface (Figure 14), the waves were associated with temporary increases in pressure, and only a 1 C drop in temperature, typical of solitary waves as opposed to bores (sustained pressure increase) and density currents (sustained pressure increase and usually large temperature decrease). Time-height sections of MPR potential temperature and water vapor mixing ratio (see Figure 15) also show the two temporary increases in the depth of the boundary layer. Again, since the vertical displacement at the profiler site is not sufficient to bring parcels to their LCL's, θ and r_v were conserved during vertical motion and serve as excellent indicators of parcel displacements. One can clearly see a temporary upward vertical displacement centered near 0400 UTC, followed by a smaller upward displacement just before 0430 UTC.

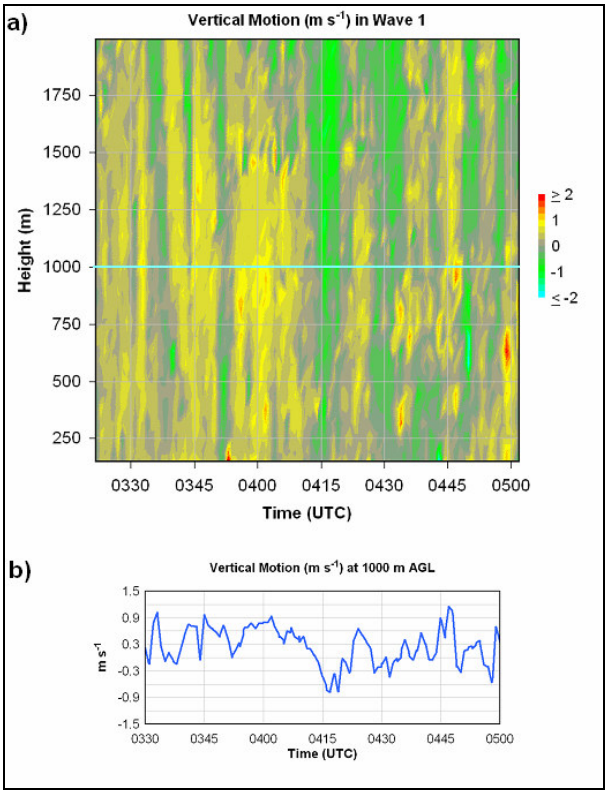

Figure 13. a) Time-height section of MIPS 915 MHz profiler vertical motion, and b) plot of vertical motion vs. time at 1000 m AGL (along horizontal blue line in a).

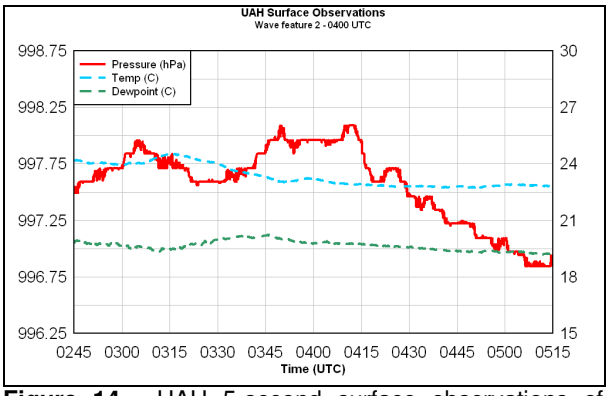

Figure 14. UAH 5-second surface observations of pressure (hPa, solid red), temperature (C, dashed blue), and dewpoint (C, dashed green), around the time of the waves around 0400 UTC.

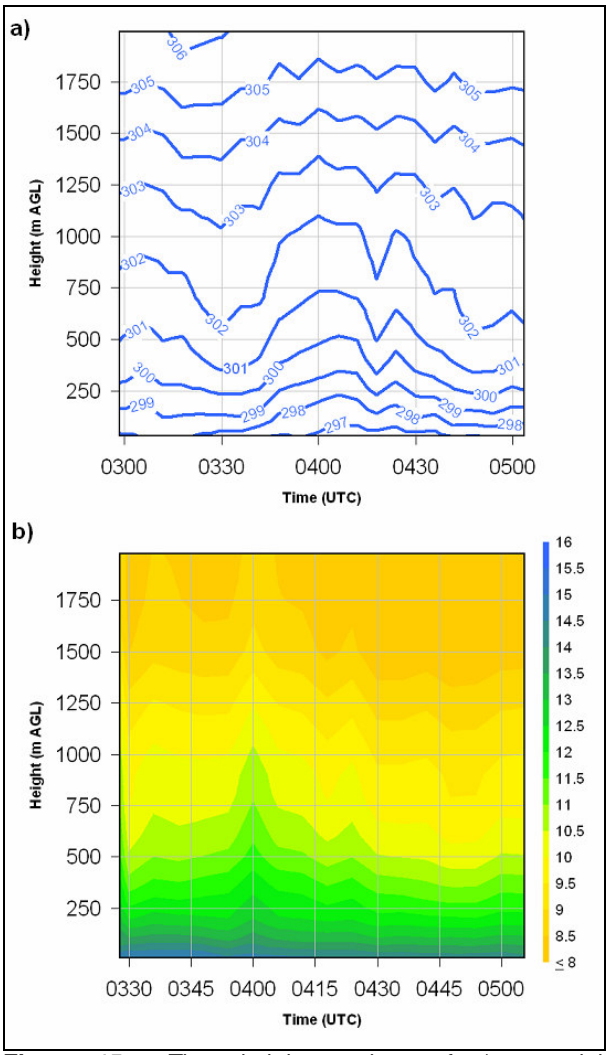

Figure 15. Time height sections of a) potential temperature (K) and b) water vapor mixing ratio (g kg^{-1}) between 0330 and 0500 UTC from UAH MPR data.

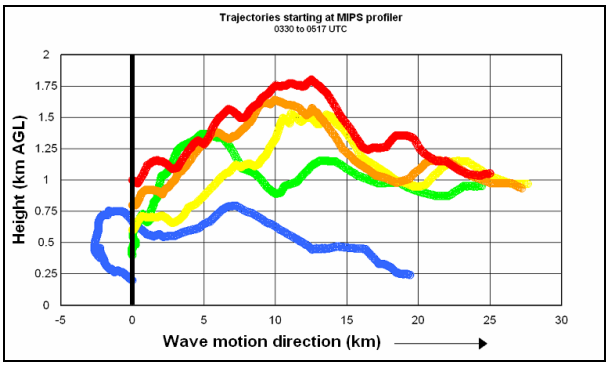

Figure 16. 2D trajectories in plane of wave motion based on TSC of profiler data at 0330 UTC. All trajectories begin at 0 km, and at 200 m AGL (blue), 400 m (green), 600 m (yellow), 800 m (orange), 1 km (red).

Assuming the wave feature was a two-dimensional phenomenon, a time-to-space conversion of 915 MHz profiler winds and vertical motion at 0330 UTC was used to produce trajectories, within a plane perpendicular to wave motion, of parcels released from 200, 400, 600, 800, and 1000 m AGL at 0330 UTC (see Figure 16). The trajectories of the air parcels were carried through 0517 UTC, with the positive horizontal direction being the same as the direction of wave motion. Note that all 5 trajectories follow at least one pattern similar to that for a solitary wave shown in Figure 4, and the 4 highest altitude ones show some evidence of the second wave in the soliton also. It is also interesting that there is some vertical spreading of the parcels. Figure 15a also shows vertical spreading of the isentropes, indicating destabilization as the wave moves through, similarly to the bore discussed in section 4a.

5. THERMODYNAMICS AND CI

As mentioned in section 4, both wave features caused upward vertical displacement, even if temporary, and destabilization. A simply examination of dry static stability (Figure 17) through the Brunt-Vaisala frequency from 0100 through 0500 UTC shows two important things. First of all, as mentioned in section 3, a low-level stable layer lies beneath a less stable layer above, providing a duct for gravity wave energy. Secondly, it should be noted that the low-level static stability (primarily below 400 m AGL) is decreased dramatically by the first wave feature around 0230 UTC, with 50 m AGL *N* dropping from near 0.030 s^{-1} to near 0.015 s^{-1} just after 0300 UTC. Then after a brief increase in *N*, to 0.021 s^{-1} at 0330 UTC, the soliton is associated with another decrease in stability, with *N* decreasing to 0.015 s^{-1} again by 0400 UTC.

However, in order to effectively quantify the effects of the passing wave features on the actual potential for convective initiation, one must use the MPR temperature and moisture profiles to examine the changes in convective inhibition (CIN, Colby 1984), cap strength, lifted condensation level (LCL), and other convective parameters. The MPR retrieves vertical

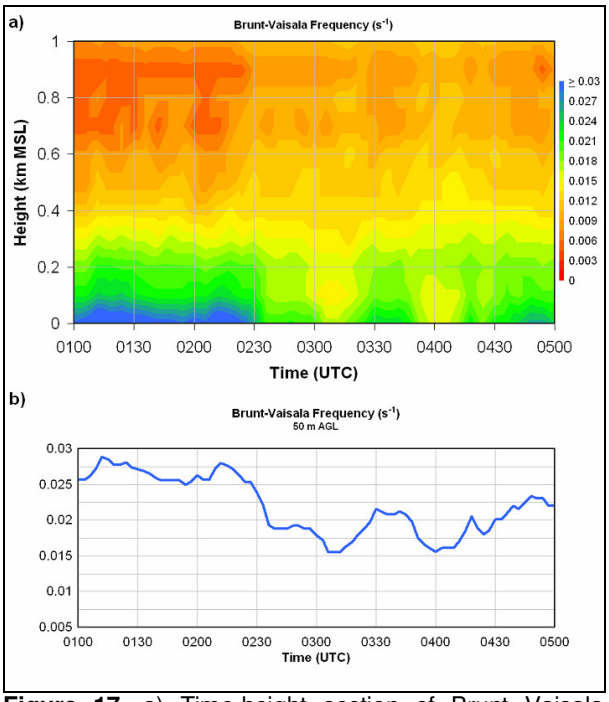

Figure 17. a) Time-height section of Brunt Vaisala frequency (s^{-1}) from MPR data, and b) time series of *N* (s^{-1}) at 50 m AGL.

profiles of temperature and water vapor every minute, allowing calculations of any thermodynamic parameters, based on any vertical level, at 1-minute resolution.

One of the primary reasons that warm-season convection often decreases dramatically after sunset is due to the radiational cooling near the surface, producing a layer of stable air that inhibits any surface-based or low-level convective initiation. The CIN is a measurement, typically in J kg^{-1}, of the potential energy associated with negative buoyancy that slows down any rising parcel, often preventing condensation or convection. The Convective Available Potential Energy (CAPE, Moncrieff and Miller 1976) is a measurement of the potential energy available for producing buoyant vertical motion once a parcel reaches its level of free convection (LFC), where the parcel is warmer than its environment and accelerates upward without additional mechanical lifting. Therefore, three basic ingredients are necessary for nighttime convection: 1) sufficient CAPE; 2) some mechanical lift; and 3) insufficient CIN to prevent a parcel from reaching its LFC and initiating convection.

In this case study, CAPE was sufficient for at least some deep convection starting from any level below 500 m AGL (Figure 18). CAPE values were gradually decreasing, typical of a nighttime situation, but were still in excess of 1,000 J kg^{-1} throughout most of the 0-500 m AGL layer, and even surface-based CAPE was 500-1000 J kg^{-1}. Therefore, sufficient instability and moisture was available in the atmosphere for convection, if a parcel could reach its LFC.

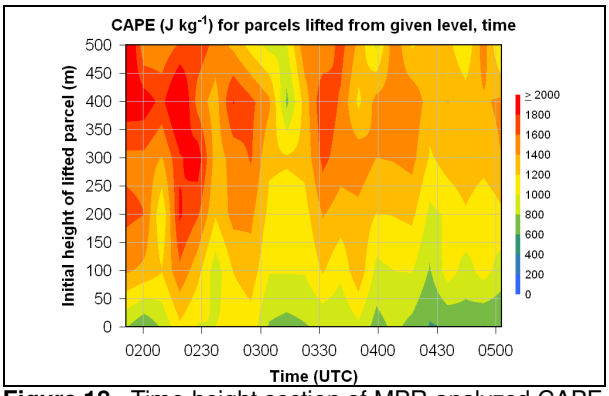

Figure 18. Time-height section of MPR-analyzed CAPE (J kg^{-1}), with the height representing the level from which the parcel is initially lifted.

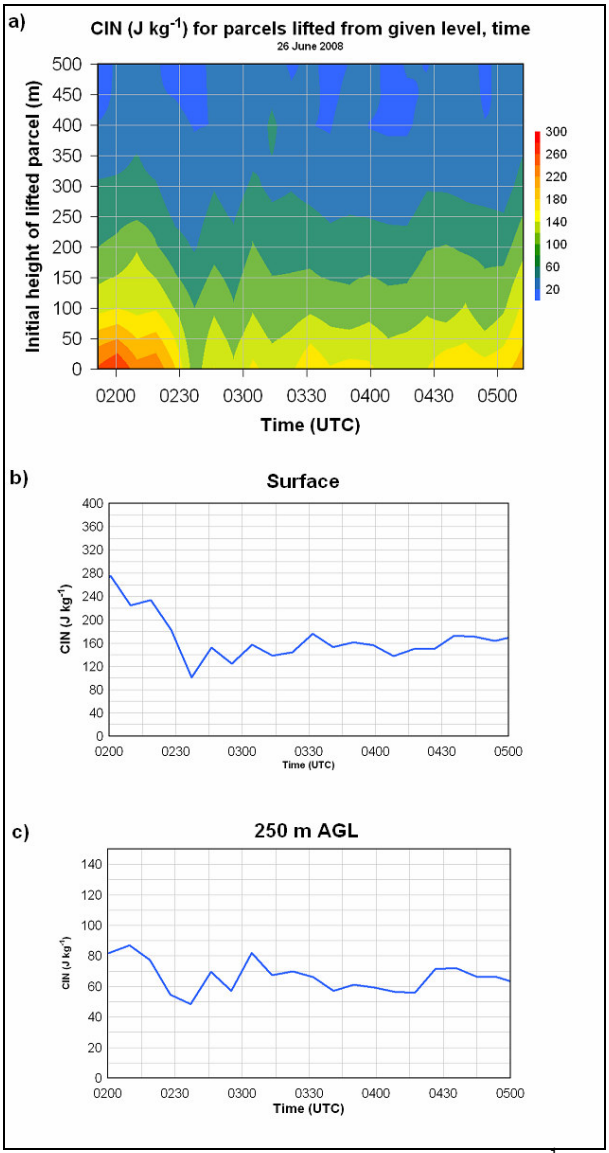

Figure 19. a) Same as Fig. 18, but for CIN (J kg^{-1}); b) CIN at surface; c) CIN at 250 m AGL

Figure 19 shows a similar time height section of convective inhibition (CIN), along with the CIN at two fixed levels, the surface and 250 m AGL. Due to the cooling and surface inversion that had formed at 0200 UTC, fairly large values of CIN had developed, especially for parcels originating at low-levels. Before the bore passed around 0230 UTC, CIN values were near 250 J kg^{-1} for parcels lifted from the surface, making it very unlikely that any parcel could reach its LFC, preventing convection at the site. However, the destabilization associated with the passage of the bore decreased the CIN quite a bit, especially below 200 m AGL, with the surface-based CIN dropping from 226 J kg^{-1} at 0217 UTC, to 101 J kg^{-1} by 0236 UTC, a drop of about 60%. CIN increased somewhat, to near 175 J kg^{-1} at 0330 UTC, then decreased again to near 138 J kg^{-1} at 0408 UTC, around the time the soliton passed by. *Therefore, the bore at 0230 UTC and the soliton at 0400 UTC destabilized the atmosphere enough to reduce convective inhibition, making it more likely that an air parcel could reach a given LFC and convective initiation (CI) could occur.*

In Figure 20, a time series of the level of free convection (LFC) for a surface-based parcel is shown. Both the bore at 0230 UTC and the soliton at 0400 UTC produced slight cooling above 1500 m AGL, and the bore passage also caused slight warming at the surface. Therefore, the LFC also lowers significantly with the passage of the bore at 0230 UTC, from 2600 m AGL to 2000 m AGL. It increases somewhat between 0300 and 0330 UTC, then decreases again, to 2100 m AGL, around 0407 UTC. So, the wave features also lowered the level of free convection somewhat, further increasing the possibility of convection.

Finally, the bores and solitary waves produced vertical motion in the lower atmosphere, that is required for convective initiation. Figures 9, 13, and 16 confirm this. While no convection occurred immediately over the MIPS site, a thunderstorm (not shown) developed at 0300 UTC about 50 km WSW of MIPS, behind the undular bore. More widespread convection developed along and just behind the soliton as it moved through northeast Alabama (see Figure 21). The soliton is also

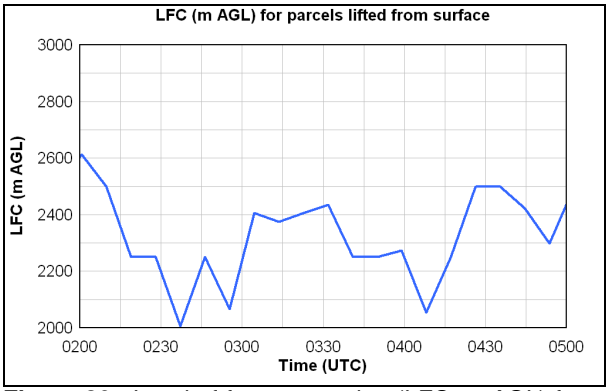

Figure 20. Level of free convection (LFC, m AGL) for a surface-based parcel.

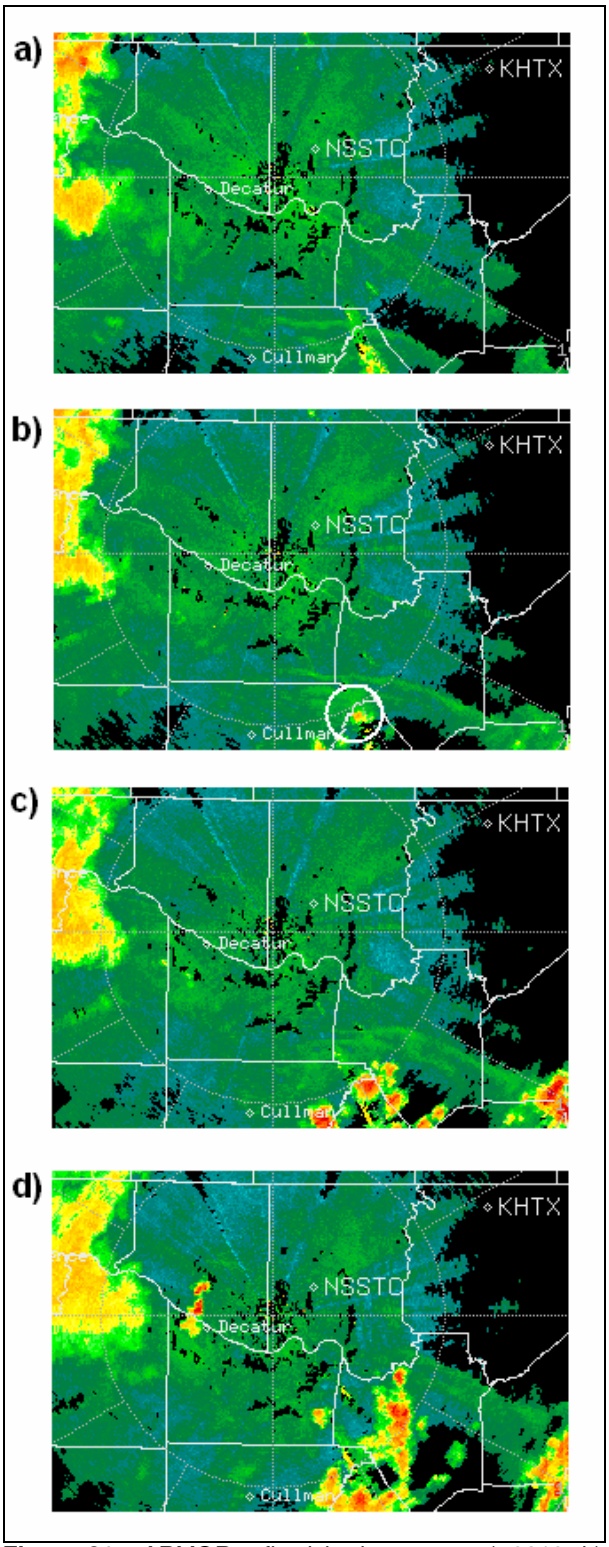

Figure 21. ARMOR reflectivity images at a) 0219; b) 0231; c) 0243; and d) 0308 UTC. The white circle in b) indicates the location of the first CI associated with the soliton.

visible as fine lines of enhanced reflectivity, likely associated with the lifting of insects by the soliton. The convection was likely enhanced by topography, and perhaps in the area of collision of the soliton with the undular bore SE of NSSTC (the location of MIPS). However, the widespread nature of the convection and its proximity to the soliton indicate that the destabilization, and possibly the lift, associated with the wave feature were largely responsible for the CI.

7. CONCLUSIONS

This study shows the kinematic and thermodynamic effects of two wave features on the NBL, using measurements from the ARMOR Doppler radar, the Microwave Profiling Radiometer (MPR) and 915 MHz profiler that are part of the UAH MIPS system, and surface data. The effects of the wave features on the convective environment are examined, and convective initiation associated with the wave features is discussed.

The first wave feature, an undular bore apparently initiated by cold outflow from thunderstorms interacting with a shallow stable layer, was shown very well by the ARMOR radar, and passed the MIPS around 0230 UTC. MIPS 915 MHz profiler measurements of vertical motion show four wavelengths of short-period upward and downward motion as the bore passed by, and MPR-derived time-height sections of potential temperature and mixing ratio show an increase in the depth of the stable boundary layer, along with a decrease in stability.

The second wave feature, a soliton or train of two solitary waves, passed the MIPS around 0400 UTC. These features were associated with longer period vertical motion, and trajectory analyses using 915 MHz profiler winds and vertical motion, assuming the waves were two-dimensional, show distinct, temporary upward displacements of air parcels, consistent with solitary waves. This feature also decreased the stability.

Basically, convective initiation (CI) requires three ingredients: a) sufficient instability (high enough CAPE and a low enough LFC), b) vertical motion, and c) a relative lack of CIN that could suppress the vertical motion of a parcel, preventing it from reaching its LFC. Since the wave features destabilize the atmosphere, they greatly reduce the CIN and decrease the LFC, both making convection more likely. *In other words, the waves lower the LFC, and also make it easier for a parcel to reach it.* A thunderstorm develops behind the undular bore, and more widespread convection develops near and just behind the soliton.

This study quantifies the effects of wave features on the convective potential of the boundary layer, by calculating the changes in commonly-used parameters such as CIN, CAPE, and LFC. It also allows for detailed analysis of the vertical displacements associated with wave features. Further study of such features in the nocturnal boundary layer are required, as they may be responsible for a large percentage of nocturnal convective events away from well-defined synoptic-scale features or low-level jets.

REFERENCES

Abdullah, A. J., 1956: A note on the atmospheric solitary wave. *J. Atmos. Sci.*, **13**, 381-387.

Benjamin, T. B., 1967: Internal waves of permanent form in fluids of great depth. *J. Fluid Mech.*, **29**, 559-592.

Boussinesq, J., 1871: Th´eorie de l'intumescence liquide appele onde solitaire oude translation se propageant dans un canal rectangulaire. *Inst. France Acad. Sci. C. R..,* Jun. 19, p. 755.

Christie, D. R., K. J. Muirhead, and A. L. Hales, 1978: On solitary waves in the atmosphere. *J. Atmos. Sci.*, **35**, 805-825.

Clarke, R. H., R. K. Smith, and D. G. Reid, 1981: The morning glory of the Gulf of Carpentaria: An atmospheric undular bore. *Mon. Wea. Rev.,* **109,** 1726–1750.

Clarke, R. H., 1972: The Morning Glory: An atmospheric hydraulic jump. *J. Appl. Meteor.*, **11**, 304-311.

Colby, F. P., Jr., 1984: Convective inhibition as a predictor of convection during AVE-SESAME II. *Mon. Wea. Rev.,* **112,** 2239–2252.

Coleman, T.A., K.R. Knupp, and D. Herzmann, 2009: The Spectacular Undular Bore in Iowa on 2 October 2007. *Mon. Wea. Rev.*, **137**, 495–503.

Crook, N. A., 1988: Trapping of low-level internal gravity waves. *J. Atmos. Sci.,* **45,** 1533–1541.

Crook, N. A., 1986: The effect of ambient stratification and moisture on the motion of atmospheric undular bores. *J. Atmos. Sci.,* **43,** 171–181.

Davis R. E., and A. Acrivos, 1967: Solitary internal waves in deep water. *J. Fluid Mech.,* **29**, 593-607.

Doviak, R. J., and R. Ge, 1984: An atmospheric solitary gust observed with a Doppler radar, a tall tower and a surface network. *J. Atmos. Sci.*, **41**, 2559-2573.

Koch, S.E., P.B. Dorian, R. Ferrare, S. Melfi, W.C. Skillman, and D. Whiteman, 1991: Structure of an Internal Bore and Dissipating Gravity Current as Revealed by Raman Lidar. *Mon. Wea. Rev.*, **119**, 857–887.

Knupp, K., 2006: Observational Analysis of a Gust Front to Bore to Solitary Wave Transition within an Evolving Nocturnal Boundary Layer. *J. Atmos. Sci.*, **63**, 2016–2035.

Lamb, H., 1932: *Hydrodynamics.* New York: Dover Publications, 738 pp.

Lindzen, R. S., and K. –K. Tung, 1976: Banded convective activity and ducted gravity waves. *Mon. Wea. Rev.*, **104**, 1602-1617.

Locatelli, J. D., M. T. Stoelinga, and P. V. Hobbs, 2002: A new look at the Super Outbreak of tornadoes on 3–4 April 1974. *Mon. Wea. Rev.*, **130**, 1633-1651.

Locatelli, J. D., M. T. Stoelinga, P. V. Hobbs, and J. Johnson, 1998: Structure and evolution of an undular bore on the high plains and its effects on migrating birds. *Bull. Amer. Meteor. Soc.,* **79,** 1043–1060.

Moncrieff, M. W., and M. J. Miller, 1976: The dynamics and simulation of tropical cumulonimbus squall lines. *Quart. J. Roy. Meteor. Soc.,* **102,** 373–394.

Nappo, C. J., 2002: *An Introduction to Atmospheric Gravity Waves*. San Diego: Academic Press, 276 pp.

Peters, A. S., and J. J. Stoker, 1960: Solitary waves in liquids having non-constant density. *Comm. Pure Appl. Math.,* **13**, 115-164.

Rayleigh, Lord, 1876: On waves. *Phil. Mag.*, **1**, 257-279.

Rottman, J.W., and F. Einaudi, 1993: Solitary Waves in the Atmosphere. *J. Atmos. Sci.*, **50**, 2116–2136.

Rottman, J. W., and Simpson J. E., 1989: The formation of internal bores in the atmosphere: A laboratory model. *Quart. J. Roy. Meteor. Soc.,* **115**, 941–963.

Seitter, K.L., 1986: A Numerical Study of Atmospheric Density Current Motion Including the Effects of Condensation. *J. Atmos. Sci.*, **43**, 3068–3076.

Simpson, J. E., 1997: *Gravity Currents in the Environment and the Laboratory.* 2nd ed. Cambridge: Cambridge University Press, 244 pp.

Tepper, M. 1950: A proposed mechanism of squall lines: The pressure jump line. *J. Meteor.*, **7**, 21-29.